The Biophysicist

Liquid–Liquid Phase Separation: Undergraduate Labs on a New Paradigm for Intracellular Organization

Caroline P. Riedstra[1], Ryan McGorty[1,*]

[1]Department of Physics and Biophysics, University of San Diego, San Diego, CA 92110, USA

ABSTRACT Recent work has shown that the intracellular environment is organized not only through membrane-bound organelles but also through fluid droplets that emerge through liquid–liquid phase separation (LLPS). Intracellular LLPS has attracted recent attention because these fluid droplets, termed *biomolecular condensates* or *membraneless organelles*, seem to play important roles in cells' responses to stress, gene regulation, and pathologies. Our understanding of intracellular LLPS has advanced through many quantitative biophysical techniques. Here, we describe a set of undergraduate lab activities that highlight these biophysical techniques. We use various optical microscopy methods and quantitative image analysis to characterize the physical properties of a model aqueous system that exhibits liquid–liquid phase separation. These lab activities can form a multiweek module that exposes students to this exciting new and interdisciplinary field that investigates how phase transitions organize the cell interior.

KEY WORDS optical microscopy and imaging; laboratory exercises; undergraduate biophysics

I. INTRODUCTION

Recently, a new paradigm for how the cellular interior is organized has spurred numerous research efforts, much of which is well summarized in recent review papers (1–21), although keeping up with the accelerating pace of discovery in this field is difficult. This new paradigm challenges the 20th century textbook view of the cell as being partitioned by membrane-bound organelles. It is now understood that within the cell are also membraneless organelles (MLOs), which are liquid droplets of biomacromolecules, typically proteins and nucleic acids, that have phase separated from the rest of the cytosol.

In the liquid–liquid phase separation (LLPS) of proteins, RNA and DNA play a role in regulating, in both time and space, gene expression (22, 23), stress response (24), signaling (25), and other biological processes. The MLOs, which result from the process of phase separation and are sometimes referred to as biomolecular condensates, may sequester and concentrate biomolecules, buffer the concentration of given molecules (26), or, through surface tension, exert physical forces within the cell to bring together regions of the genome (27–31) or shape the cell membrane (32). While the biological significance of protein condensation (e.g., in the formation of cataracts) (33) and of two-dimensional LLPS in lipid membranes (34)

"*" corresponding author

Received: 7 January 2019
Accepted: 29 October 2019
Published: 14 February 2020

have been understood for decades, only within the last 10 y have researchers focused on LLPS as an organizing principle for the cell interior.

The recent surge in interest in liquid–liquid phase separation in the context of cellular organization is evidenced not just by research articles but by conferences (35), symposium talks (36), and the interest of drug companies (37). This interest presents an excellent opportunity to expose undergraduate physics and biophysics students to cutting-edge research and to highlight the importance and relevance of thermodynamics, fluids, and optics. Understanding the properties, function, and formation of these MLOs or liquidlike condensates seen in cells requires an interdisciplinary approach. Thermodynamics lays the foundation for us to describe the necessary conditions and driving forces for LLPS (17). Models from the field of polymer physics capture essential features of LLPS with a minimum of parameters (4, 20). From the fields of fluid dynamics and soft matter physics, we borrow tools to understand the material properties of these MLOs (38). Biochemistry helps us predict what sequences of amino acids or of nucleotides will lead to the weak multivalent molecular interactions that promote LLPS (39–42). Finally, optical methods allow us to both observe MLOs and, in combination with genetic engineering, controllably induce intracellular LLPS (8).

The necessity of applying knowledge from different scientific fields to fully understand biological LLPS makes this an excellent topic for undergraduate students. It allows students to integrate concepts from multiple disciplines, to not compartmentalize ideas inside disciplinary silos, and to develop an appreciation for the field of biophysics—a field often only presented to undergraduate students at a superficial level. Therefore, we describe here a recently developed biophysics laboratory module on the topic of LLPS.

The labs and other class material we have developed are used in an upper division course on experimental biophysics that is required for students completing our biophysics major, a major we began in 2012. Students spend about 5 wk on this LLPS module doing the activities we describe below. In the other half of the semester, students work on a lab module inspired by Appleyard et al. (43), where they build, calibrate, and use an optical trap. The class meets for a total of 5 h each week, including both a lecture and a laboratory component. However, students typically spend much more time outside of class completing experiments and analyzing data. We have taught this lab module as described three times, first in the spring of 2016 and with improvements made after each iteration. Therefore, we have yet to assess long-term outcomes for students who have completed this module. However, students have reacted positively overall to the lab module and have commented that it balances well with the instrumentation-heavy module on optical tweezers.

II. BACKGROUND ON THE THERMODYNAMICS OF PHASE SEPARATION

A number of excellent papers review the field of biomolecular LLPS, including a few that emphasize concepts from physics (4, 10, 17, 19). Here, we will not review the physics of LLPS in the detail contained in such papers, but we will highlight some important concepts suitable for discussion in an undergraduate physics or biophysics course.

We refer to LLPS as the reversible process that leads an originally homogeneous liquid to demix into two distinct fluid phases. This process is thermodynamically favored if it results in a decrease in the free energy F. Therefore, to begin understanding the thermodynamics of phase separation, we look at the free energy as a function of the sample's composition. The free energy density of a solution containing a certain volume fraction ϕ of some solute may appear convex with a single minimum, as shown in Figure 1A. Although a system is inclined to minimize its thermodynamic potential, given that new solute molecules cannot spontaneously appear or disappear (i.e., the number of molecules is a conserved quantity), the system would be

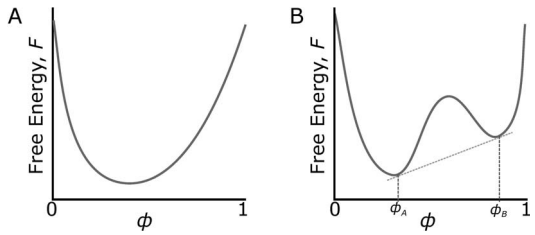

Fig 1. Free energy versus the volume fraction. (A) Phase separation would not occur in this case. (B) A miscibility gap exists in which phase separation will occur.

unable to lower its free energy. If, however, the free energy as a function of composition is not convex, like that shown in Figure 1A, but is concave over some region (i.e., $\partial^2 F/\partial\phi^2 < 0$), as seen in Figure 1B, then it may be able to lower its free energy (3, 44) by splitting into two phases, each having a different volume fraction. If the initial composition was ϕ_0, it may separate into phase A, having composition ϕ_A, and phase B, having composition ϕ_B, provided the lever rule is satisfied where the fraction of the sample volume in phase A is x and $\phi_0 = x\phi_A + (1-x)\phi_B$. This demixing will be thermodynamically favored if $F(\phi_0) > xF(\phi_A) + (1-x)F(\phi_B)$, which may be possible for the situation in Figure 1B but certainly not for that in Figure 1A (44).

Multiple theoretical approaches can be used to find a thermodynamic potential, which is a function of sample composition (10). A fairly simple mean field lattice model that is widely used to understand polymer systems and has been recently used to study intracellular LLPS (45–47) is the Flory–Huggins model. With this lattice model, the free energy density (free energy per unit volume) of mixing polymers of length N in some solvent can be shown to be $f = k_B T[(\phi/N)\ln\phi + (1-\phi)\ln(1-\phi) + \chi\phi(1-\phi)]$. The first two terms in this expression represent the entropy of mixing and always promote mixing. The last term is the interaction free energy and depends on the interactions between polymers and solvent molecules, which are embedded in χ, the Flory parameter.

If χ is large enough, then for a range of ϕ, a portion of $f(\phi)$ will have negative curvature, like the curve in Figure 1B. That there is a region where $\partial^2 f/\partial\phi^2 < 0$ indicates that for certain concentrations, phase separation will occur. When phase separation proceeds, two regions will coexist, one of composition ϕ_A and one of ϕ_B, such that $(\partial f/\partial\phi)|_{\phi=\phi_A} = (\partial f/\partial\phi)|_{\phi=\phi_B}$ or, equivalently, such that the chemical potentials are equal in both phases. If a sample contains an overall composition between ϕ_A and ϕ_B, a region referred to as the miscibility gap, then phase separation will occur through one of two mechanisms. If the system is unstable, where $\partial^2 f/\partial\phi^2 < 0$, then phase separation proceeds spontaneously in a process termed *spinodal decomposition*. If within the miscibility gap $\partial^2 f/\partial\phi^2 > 0$, then the system is metastable and phase separation occurs through a process termed *nucleation and growth* (44). Few studies have explored the dynamics of LLPS within living cells, but among the few is recent work at the interface of physics and biology that applies classical nucleation theory to protein aggregation in living cells (48).

We have written an interactive Python program with a Jupyter Notebook that allows students to explore the Flory–Huggins model of phase separation (49). One can adjust the Flory parameter and the chain length of the model polymers and see the change in the free energy landscape and the resulting phase diagram. This program also allows students to understand how $f(\phi)$ and its first and second derivatives are used to construct the phase diagram. More details are included in the Supplemental Material.

III. MODEL SYSTEMS FOR STUDYING LLPS

The processes of developing, using, and refining models pervade all sciences. As David Hestenes wrote, "in science, 'modeling is the name of the game'" (50). Scientists use models to make predictions and explain phenomena. Models provide an abstract or simplified representation that allow us to communicate ideas and make sense of the world. Given the importance of modeling in science, calls have been made to build students' skills in working with and their knowledge regarding models

Table 1. Models used to understand intracellular liquid–liquid phase separation.

	Model system	
	Flory–Huggins	**Mixture of gelatin and dextran**
Model objective	Predict the state of polymer mixtures dependent on volume fraction and an interaction parameter	Allow investigation of properties of demixed fluid systems with some control over viscosity and surface tension
Assumptions	Mean-field approach with few input parameters can model intracellular LLPS	System will have similar properties to intracellular liquid–liquid systems
Representation	Equations and plots	Images and videos acquired through microscopy of the physical system
Limitations	Intermolecular interactions simplified with a single parameter that is independent of composition	System is studied in vitro, and its state cannot be altered in situ
Refinement	Use extensions to account for electrostatic interactions (e.g., the Overbeek and Voorn extension)	Confine gelatin–dextran system in droplets or alter system to respond to stimuli such as temperature
Validation	Observation of phase separation depending on concentration and on molecular interactions	Properties, such as viscosity and surface tension, that are similar to intracellular liquid droplets

(51, 52). Therefore, we make explicit to students the usage of models in our module on LLPS. We also hope that using multiple models to understand intracellular LLPS can act as a "bridge" between different disciplinary approaches, particularly those of physics and biology (53).

One model emphasized in our lab module is the previously described Flory–Huggins models. Like many other models in physics, we can represent this one with an equation. It greatly simplifies a system that may phase separate but still allows us to make predictions. We provide students with examples of how this model has advanced our understanding of intracellular LLPS. For example, Nott et al. (47) used the Flory–Huggins model to find the interaction parameter of a given protein in water.

The other model, on which students spend even more time working, is a model *system*, which consists of an aqueous solution of gelatin and dextran. This model system is much different from the Flory–Huggins model, in that rather than being represented mathematically, it is a physically realizable model that can act as a stand-in for the phase-separated intracellular environment. Although quite different from the Flory–Huggins model, it also serves to further our understanding of intracellular LLPS. Like the Flory–Huggins model, it simplifies reality: rather than working with actual cells containing numerous species of biomolecules, we use only two biopolymers. Although simplified, this model system still exhibits LLPS for certain concentrations and allows us to make predictions. For example, we can use it to predict how the size of membraneless organelles will affect how quickly they coalescence and how a system's position on the phase diagram will affect the physical properties of the demixed fluids.

Because we see great value in highlighting the different approaches to modeling intracellular LLPS, we have described the two models explained in Table 1 that we were inspired to develop from Hoskinson et al. (53). The table describes features particular to the two models, but it is not meant to be exhaustive. Both models carry additional assumptions, representations, and limitations and may be used for other objectives. Bringing such attention to these models will enhance students' understanding of the commonalities and differences in modeling used in multiple disciplines and raise their "meta-modeling knowledge" (54, 55). It is important to recognize that not all instances of LLPS can be modeled by the Flory–Huggins theory. Likewise, the intermolecular interactions in our aqueous mixture of gelatin and dextran and its physical properties are not precisely mirrored in many systems of intracellular LLPS. Nonetheless, in many cases researchers in the field of intracellular LLPS have turned to the Flory–Huggins model (3, 4, 45, 47) or to aqueous two-phase systems similar to our gelatin–dextran model system (56–58).

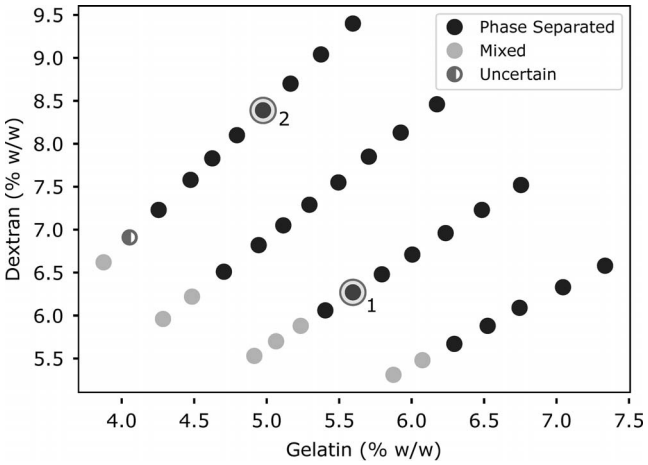

Fig 2. Phase diagram showing samples that have phase separated (dark gray) or have not (light gray). Two samples are circled because we present data from those samples in the text. We refer to these as sample 1 and sample 2.

IV. LAB MODULE ON LLPS

Here, we describe the components of our lab module on the topic of LLPS. In our experimental biophysics course, students complete each of the described tasks. However, each component could possibly be undertaken in isolation in a lab or lecture course.

We describe the lab components in the order in which we have students undertake them. First, students are given gelatin and dextran solutions to mix together and to observe what happens, resulting in the construction of a phase diagram. Then, typically in the same 3-h lab session, students are introduced to the optical microscope that will be used in all subsequent labs. In those labs, students observe droplets coalescing, perform fluorescence recovery after photobleaching experiments, and track single colloidal particles within droplets. Those labs and the associated data analysis are carried out over the remaining 3–4 wk of this module.

A. Constructing a phase diagram

One of the first tasks students undertake is the creation of a phase diagram such as that shown in Figure 2. This task acquaints students with the experimental model system used and introduces students to lab skills such as pipetting, making serial dilutions, practicing sterile techniques, and recording observations in a lab notebook. We provide students with prepared aqueous solutions of 500 kDa dextran (Spectrum Chemical D1004, New Brunswick, NJ; ∼19% by weight) and of cold-water fish gelatin that is liquid at room temperature (Sigma-Aldrich G7041, St. Louis, MO; ∼12% by weight). Students then make a series of samples containing various concentrations of the two components. After mixing by hand, students may observe whether phase separation occurs or not by visual inspection. Holding the sample up to a light, samples that have phase separated appear cloudy or opaque, whereas those that have not are transparent. Many students are surprised when they observe a phase-separated solution, just like oil and water, after mixing together aqueous solutions.

After constructing their own phase diagram, students may consult published phase diagrams for similar systems (59, 60) and compare the general shape with phase diagrams of biomolecules [e.g., see Li et al. (25, fig 4) or Elbaum-Garfinkle et al. (61, fig 1)]. With a constructed phase diagram, students may be led to consider the concepts of tie lines and of how the composition of the two phases depends on the overall concentration of the sample. These concepts will resurface through the lab module as students investigate the physical properties of samples at different locations within the phase-separated region of the phase diagram.

In certain cases, it may be difficult to determine whether phase separation has occurred with the naked eye. In such cases, observing the system under a microscope is useful.

B. Optical microscopy methods

Much of the research in this field has been conducted with optical microscopy. Thomas Montgomery (62), writing in 1898, used a Zeiss light microscope to observe that the nucleolus "may be either fluid or viscid in consistency" and that "in the great number of cases it has no limiting membrane." More than 100 years later, students and instructors at the Woods Hole Marine Biological Laboratory using more advanced optical microscopes again noted the

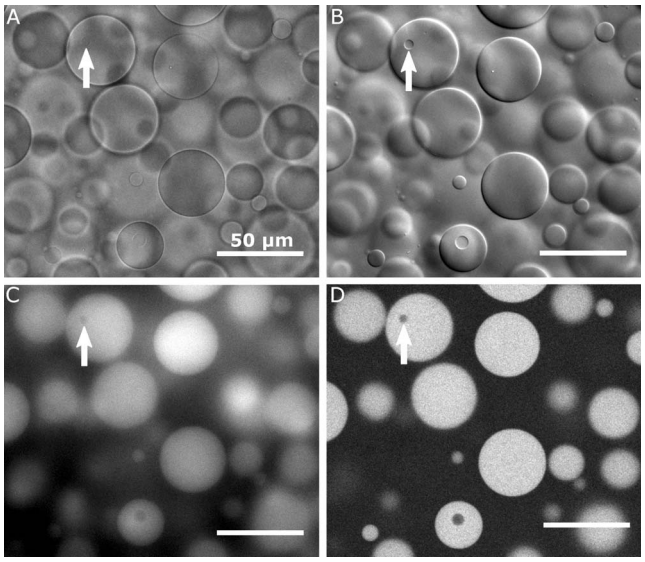

Fig 3. A gelatin–dextran mixture containing gelatin-rich droplets with a dextran-rich continuous phase imaged with a 20× objective. Rhodamine dye, which preferentially enters the gelatin-rich phase, has been added to allow for fluorescence imaging. Images of the same region of this sample are shown with different microscope modalities: (A) brightfield, (B) differential interference contrast, (C) widefield fluorescence, and (D) laser-scanning confocal microscopy. The arrow points to the same droplet-within-droplet; that it is barely visible in brightfield and widefield fluorescence emphasizes the benefit of contrast-enhancing techniques.

liquidlike behavior of subcellular organelles (63). That discovery led to work published in 2009 (64) and ushered in many other studies on LLPS forming membraneless organelles, most of which utilize optical microscopy.

In general, covering optical microscopy techniques—particularly how they are used for biological or medical purposes—provides a great way to present relevant applications of many physical concepts (65). In particular, discussing how one can image *transparent* objects, which is often required in biological studies and is the case for our demixed system, brings with it several important concepts (e.g., the distinction between contrast and resolution, refractive index, diffraction, and interference). When observed under bright-field microscopy (Fig 3A), there is little contrast between the droplet phase and the continuous phase (these corresponding to either the dextran-rich or gelatin-rich phases depending on the overall sample composition). Moving a droplet slightly out of focus improves contrast. However, a better method of enhancing contrast is with differential interference contrast (DIC; Fig 3B) or phase contrast.

Given that the microscope we primarily used was equipped with DIC, we focus on that technique. DIC is enabled by first splitting the transmitted illumination light into two orthogonally polarized beams, which are slightly spatially separated from one another along what is termed the shear axis. After passing through the sample, those sheared orthogonally polarized beams are recombined with a prism and passed through a polarizer. Relative phase shifts of the two orthogonally polarized beams because of regions of different refractive indices within the sample will result in the recombined beam being elliptically polarized. The amount of light passing through the final polarizer will depend on the degree of ellipticity. In this way, differences in phase of the light rays passing through the sample are converted into differences in intensity. DIC imaging provides contrast that depends on the gradient of the optical path length along the *shear axis* (66).

In addition to imaging with transmitted light, students also explore fluorescence microscopy. We add a small amount of rhodamine dye to the gelatin and dextran samples, and the dye preferentially enters the gelatin-rich phase. Students first perform wide-field fluorescence imaging (Fig 3C). Typically, the contrast is poor with this imaging modality, especially when there is a high density of fluorescently labeled gelatin-rich droplets in the sample. Students then switch to laser scanning confocal microscopy (Fig 3D). Confocal microscopy provides much higher contrast between the two phases. In the confocal imaging mode, a focused laser spot is scanned through the sample, and emitted light passes first through a pinhole and then onto a detector. With the pinhole conjugate to the laser spot, only emitted light originating from that spot in the focal plane will pass through, greatly reducing out-of-focus light. This process provides optical sectioning and allows for clear images of fluorescently labeled droplets (67). Although we have used samples with fluorescent dye to allow students

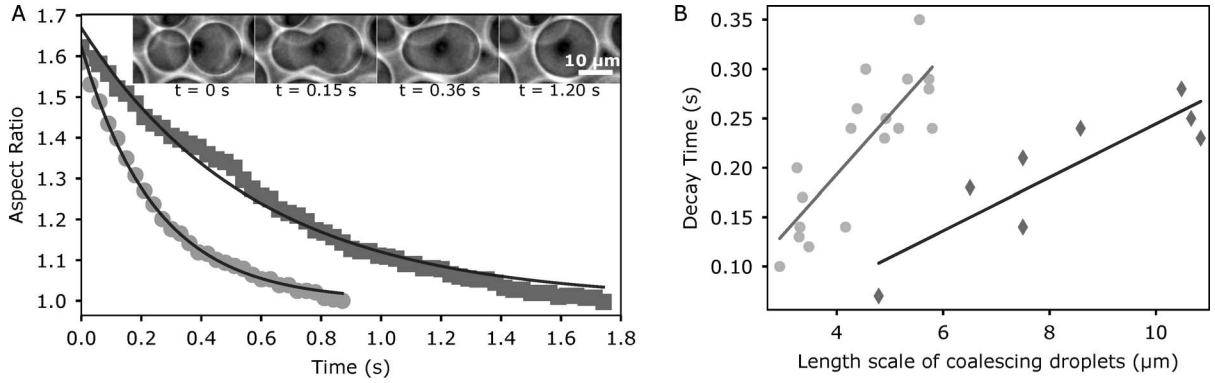

Fig 4. (A) Samples corresponding to points 1 and 2 on the phase diagram in Figure 2 were imaged by a 20× objective at 33 Hz. We measure the aspect ratio by fitting the fusing droplets to an ellipse and calculating the ratio of the length of the long axis to that of the short axis as described in Elbaum-Garfinkle et al. (61). By fitting the aspect ratio as a function of time to an exponential function, we extract a characteristic decay time. Here, we find a decay time of 0.58 and 0.25 s for samples 1 (darker squares) and 2 (lighter circles), respectively. For the coalescence events analyzed in the two samples, the size of the coalescing droplets was about the same. A sequence of images from the movie analyzed for sample 2 is shown as an inset. (B) We plot the characteristic decay time versus the length scale of the coalescing droplets to estimate the capillary velocity. The characteristic length scale is defined, as in Elbaum-Garfinkle et al. (61), as $[(l-w)w]^{1/2}$, where l is the long axis and w is the short axis of the ellipse fit to the coalescing droplets. We find capillary velocities on the order of 10 μm/s.

to compare microscopy modalities and to perform fluorescence recovery after photobleaching experiments (as described later), it may also be possible to have students quantify the fluorescent signal in both the droplet and continuous phases to calculate a partition coefficient, as has been done to study intracellular bodies (68).

When we have taught this lab module, we have relied primarily on a Nikon A1 microscope in a shared imaging facility on campus and used 20× 0.75 NA and 60× 1.40 NA objectives. During the first lab session of this LLPS module, students are guided through the components of the microscope because, for many, it is the first time they have used such a research-grade instrument.

C. Observing droplet coalescence

After gaining familiarity with the microscope, students acquire videos of droplets coalescing, which entails mixing up a solution that will phase separate, shaking vigorously, loading a few microliters of the sample into a glass slide, and imaging before the two phases separate completely into two layers. Once two droplets make contact and start to merge, they will progress toward a spherical shape to minimize surface area. The rate at which the coalescing droplets proceed to a spherical shape depends on the surface tension and on the viscosity. The greater the surface tension, the faster coalescence will occur. The greater the viscosity, the slower it will occur. The ratio of the surface tension to the viscosity is termed the *capillary velocity*. By quantitatively analyzing droplets coalescing, students are able to find an estimate of this capillary velocity. Students are then asked to compare their values with capillary velocities reported in the literature on intracellular LLPS, where such velocities range from ∼0.01 μm/s to nearly 10 μm/s (61, 69).

To estimate capillary velocity quantitatively, we analyze videos of coalescing droplets with ImageJ, an open source software commonly used for biological image analysis (70). For each video, students measure the aspect ratio of merging droplets in each frame. Typically, by imaging at 5–40 frames per second with a 20× objective, we can clearly observe the coalescence process of ∼3–100-μm-diameter droplets over tens of frames. The aspect ratio of coalescing droplets decays exponentially with time until it reaches a value of 1, indicating a circular shape. The aspect ratio versus time is fit to an exponential function to extract a characteristic decay time (Fig 4A). This fitting is done for several drop–drop coalescence events

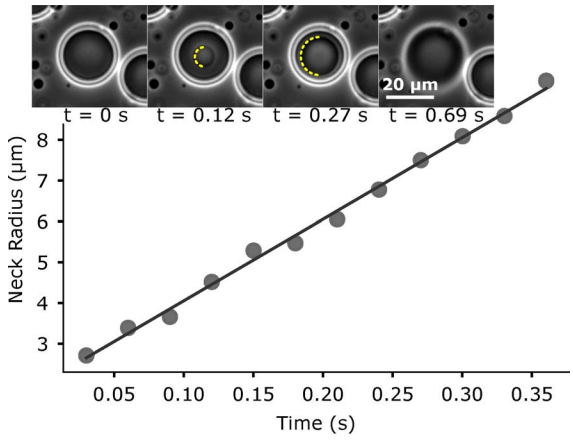

Fig 5. A gelatin-rich droplet rises to the top of the sample chamber and coalesces with the wetting layer. Here, we use a phase-contrast microscope to observe the neck form between the droplet and the planar interface of the wetting layer; however, we can also observe the neck by differential interference contrast. We observe that the radius of the neck grows linearly with time. The inset shows images where a yellow semicircle highlights the neck that forms between the wetting layer and the droplet.

featuring droplets of various sizes (although, we found it best if the two droplets coalescing are originally of nearly equal size). Once all videos are analyzed to extract the characteristic time to achieve a spherical shape, a plot of that time versus the length scale of the fusing droplets should display a linear trend, with the slope being approximately equal to the inverse capillary velocity (Fig 4B) (71). This process is then repeated for another one or two samples made with a different overall composition.

In addition to observing two droplets coalesce, it is also possible to catch instances of droplets sedimenting or creaming (because of the density difference between the two fluid phases) and then proceeding to coalesce at a planar interference formed from a wetting layer on the glass slide or coverslip. We have found that it is usually the gelatin-rich phase that wets the glass. When a droplet coalesces with the wetting layer, it is possible to observe the neck, which connects the droplet to the wetting layer, form and grow (Fig 5) (72). The growth of the radius of that neck is expected to be linear in time and, like the coalescence of two droplets, proportional to the capillary velocity.

We note that the linear relationship between either droplet size or neck radius and time is only valid for the regime where the Ohnesorge number (Oh) is less than or approximately 1. The dimensionless Oh is the ratio of the viscous force to the inertial and surface tension forces. For situations where, compared with our system, the viscosity is much smaller, the surface tension much greater (e.g., in the case of water droplets coalescing in air), or both, then a length scale that grows with the square root of time may be observed (73, 74). However, liquid droplets observed in cells may be ∼1000 times more viscous than water and have surface tensions $\sim 10^5$ smaller than that between air and water (64). Therefore, Oh will safely be much less than 1. Such large viscosities and low surface tensions are expected in fluids made up of a dense collection of macromolecules. In particular, scaling arguments predict the surface tension to scale as $k_B T/L^2$ where k_B is the Boltzmann constant, T is the temperature, and L is the length scale of the molecule making up the fluid (64). Therefore, for liquids comprising biomacromolecules that are ∼100 times larger than simple molecules, like water, one may expect surface tensions to be $\sim 10^4$ times smaller.

We have directed students toward observing the coalescence of two droplets rather than one droplet with a wetting layer. However, either method allows students to estimate the capillary velocity. Students do so for multiple samples. Students should find that the capillary velocity does depend on the sample composition. For example, we see that the capillary velocity differs by a factor of about 2 for the two samples shown in Figure 4A. This presents a good opportunity to challenge students to think about why the capillary velocity is changing and whether that is due to a change in viscosity, in surface tension, or in both. The next two components of the lab module allow students to address this issue.

D. Performing fluorescence recovery after photobleaching experiments

After conducting fluorescent imaging experiments on their samples, students will be familiar with the concept of photobleaching.

When fluorescent molecules photobleach, they chemically change in a way that causes them to fluoresce no longer. Imaging for prolonged times or at high illumination intensities increases the fraction of photobleached molecules. In most imaging experiments, one works to minimize photobleaching. However, students next conduct experiments that take advantage of the phenomena of photobleaching.

Photobleaching can be put to good use by allowing us to further measure the material properties of our fluorescently labeled fluid phases through the application of a technique known as fluorescence recovery after photobleaching (FRAP) (75). FRAP experiments are conducted by first bleaching a small region of the fluorescently labeled phase and then measuring the recovery of fluorescence intensity in that region. Fast recovery indicates that the fluorescence molecules can quickly diffuse, indicating a lower viscosity fluid. Slower recovery would indicate a more viscous solution, and little or no recovery indicates a solid or viscoelastic material instead of a fluid.

After completing the previous two lab activities, students are familiar with the operation of the Nikon A1 and can learn to use the FRAP features. The time and laser power needed to bleach a small region, the framerate at which to observe recovery, and the total time to observe recovery can all be varied. Once students find the optimal values for these parameters, they take FRAP measurements on fluorescently labeled droplets from multiple samples.

After data acquisition, students analyze the images to extract the characteristic recovery time, as shown in Figure 6. Theoretical models for the recovery curve depend on the geometry of the bleached region and other factors (76–78). However, it is often the case that a simple phenomenological model of a single exponential is used (25, 61, 79, 80). We have students fit their measurements of fluorescence recovery to a single exponential function to make the analysis and corresponding code as simple as possible. However, in future semesters we may turn to freely available software capable of using more sophisticated recovery models (81).

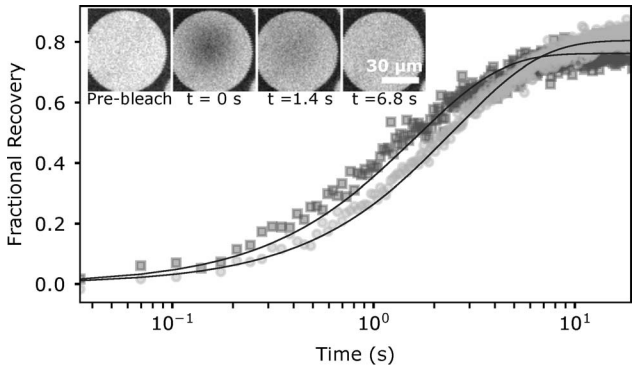

Fig 6. Fluorescence recovery after photobleaching experiments on fluorescent gelatin-rich droplets with a 20× objective and imaging at 28 Hz. We measure how the intensity recovers after photobleaching to extract a characteristic recovery time. Here, we find recovery times of 1.6 and 2.5 s for the samples labeled 1 (darker squares) and 2 (lighter circles), respectively. The slower recovery of sample 2 indicates that it is the more viscous of the two. Images of a droplet from sample 1 before and after the bleaching process are shown in the inset.

As with the previous lab activity, students repeat FRAP experiments with multiple samples to discover how the determined fluorescence recovery time depends on sample composition. Because the recovery time is proportional to the viscosity, students can begin to resolve the issue posed at the end of the last section regarding why the capillary velocity changes with sample composition and whether that stems from changes in viscosity, surface tension, or both. For example, by comparing the two recovery curves in Figure 6, we see that sample 2 is about 1.5 times more viscous than sample 1. From analyzing drop–drop coalescence events, we found earlier that sample 2 had a capillary velocity approximately twice that of sample 1. Therefore, because capillary velocity is the ratio of the surface tension to viscosity, we can conclude that the surface tension of sample 2 is approximately 3 times greater than that of sample 1.

Students are led to find that it is difficult to determine the precise viscosity of the sample through FRAP measurements. In many published works, the conclusion to FRAP experiments is a report of an "apparent" diffusion coefficient for the fluorescent molecule. This apparent, as opposed to precise, diffusion coefficient is found because simplifying as-

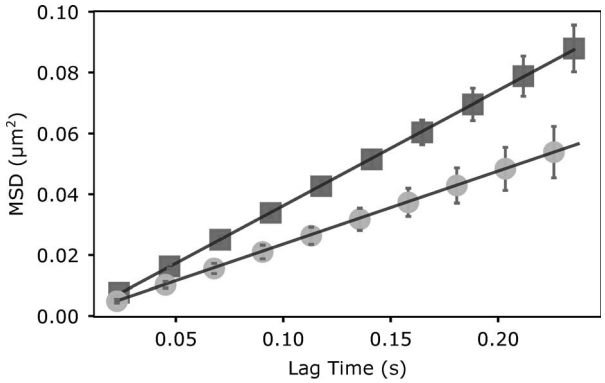

Fig 7. Particles tracked within droplets of the gelatin-rich phase. From particle tracking, we find the two-dimensional mean squared displacement (MSD) as a function of time lag t to determine the diffusion coefficient D from MSD $= 4Dt$. Here, we show the MSD for samples 1 (darker squares) and 2 (lighter circles). We see that the diffusion coefficient is greater for sample 1 (0.095 $\mu m^2/s$) compared with that for sample 2 (0.060 $\mu m^2/s$). This supports the data from fluorescence recovery after photobleaching for these two samples, which indicated that sample 2 had the more viscous gelatin-rich phase.

sumptions are typically made in the data analysis. Furthermore, the hydrodynamic size of the fluorescent molecule must be known if one is to calculate the viscosity. Therefore, while students can quantitatively compare the relative viscosities of different samples, they do not find a precise absolute value for the viscosity. However, that can be accomplished in the next activity.

E. Tracking single particles

Lastly, students conduct single-particle tracking experiments on the gelatin and dextran sample. A small number of 200-nm-diameter fluorescent polystyrene beads are added to a sample. We have found that these beads prefer the gelatin-rich phase. By tracking the beads, students can find their mean squared displacements (MSDs) as a function of lag time, as shown in Figure 7. From such MSD data, students determine the bead's diffusion coefficient and, from that, determine the viscosity of the gelatin-rich phase.

Because multiple articles have already detailed, the tracking of Brownian particles in regard to its theoretical underpinnings, its practical issues, and ways to implement it in an undergraduate lab (82–84), we will not do so here. We have found that this last lab activity is not always feasible to complete in the time allotted to the LLPS module. However, if time does permit, single-particle tracking offers a way for students to measure precisely the viscosity of the samples. With values for the measured viscosities, students can then find a quantitative estimate for the surface tension from the measured capillary velocities. For example, from the data presented in Figure 7, students can determine that the viscosity of samples 1 and 2, as indicated in Figure 2, are approximately 23 and 36 mPa·s, respectively. Together with the earlier measurements of the capillary velocity, we find a surface tension between the gelatin-rich and dextran-rich phases of approximately 0.1–1 μN/m. We note that precise values for the surface tension cannot be extracted given that our measurements of droplet coalescence provide only an estimate of the capillary velocity. Our estimated surface tension is within the range of surface tensions found in intracellular liquid droplets of 0.1–10 μN/m (61, 69, 71).

V. VENUES

We implemented these activities in an upper division experimental biophysics course that combined lecture and lab. However, components could also be used in the following courses:

1. Lecture. Although it may not be possible to convert the previously described lab activities into classroom demonstrations, the concepts of LLPS and how they play a role in cellular organization could still be discussed. In particular, for courses on statistical mechanics or on biophysics, a class could be spent on lattice models like the Flory–Huggins model and how they are being used to better understand intracellular organization. In a lower division course, this could be used to highlight the value of interdisciplinary approaches, as has been done for other soft matter topics (85).
2. Fluids. The activity on observing coalescence could be used as an isolated lab in a fluids course, with or without making connections

to LLPS or MLOs. With samples already prepared and access to an optical microscope, students would require only an hour or two to record and start analyzing coalescence events. Students could then be led, with guidance, toward relating the time scale of coalescence, droplet size, viscosity, and surface tension through dimensional analysis.

3. Optics. Underlying the confocal microscopy and differential interference contrast are several important concepts in optics, including resolution and contrast, fluorescence, polarization, and interference. The gelatin and dextran sample used here provides an excellent system for showcasing both imaging modalities given that rhodamine dye prefers one phase over the other and that the two phases are close in refractive index.

VI. CONCLUSION

We have developed a lab module consisting of several activities: mixing together aqueous gelatin and dextran solutions in various concentrations to develop a phase diagram; using various microscope modalities to observe gelatin-dextran emulsions; quantitatively analyzing droplets coalescing to estimate the capillary velocity; employing FRAP to measure an apparent diffusion coefficient; and conducting single-particle tracking experiments to measure viscosity. Through such labs, students gain familiarity with a number of techniques and tools commonly used in experimental biophysics labs. Moreover, students learn about the recent work to understand membraneless organelles and how LLPS helps to structure the cellular interior.

We have also described how different models can be used to understand intracellular LLPS. However, students may benefit from an additional discussion of how certain models can potentially hinder our understanding of this topic. For instance, take the structure–function paradigm prevalent in molecular biology. According to this model, a protein's structure dictates its function. Therefore, intrinsically disordered proteins that lack a well-defined structure are not viewed as functionally important. However, such disordered proteins are now recognized as key players in intracellular LLPS. As another example, take the viewpoint that it must be active processes that give order to the cell because thermodynamics tells us that, otherwise, disorder will prevail. However, with our current understanding of intracellular LLPS, we now know that cells can compartmentalize and structure their interior by thermodynamically driven processes. Finally, there is the textbook model of cellular organelles all being membrane-bound, which is certainly not the case. That all these models have been challenged by discoveries over the last decade showcases the constant refining process through which models go.

We conclude by highlighting some of the outstanding questions in this field (11). We found that discussing these open questions with students is highly motivating because they see their work in lab as relevant to cutting-edge research. One question concerns how the cell maintains multiple MLOs that do not Ostwald-ripen into one single large droplet. Another is what types of molecular interactions lead to LLPS within cells and how cells modulate those interactions. Finally, it is known that many neurogenerative diseases are associated with protein aggregates and that many of the proteins making up those aggregates are prone to LLPS. However, the connection between LLPS and pathological aggregates is unclear (16).

We hope that these laboratory activities can be used to bring current biophysics research into the undergraduate curriculum. The detailed set of experiments can be used as described or rearranged to fit within a variety of physics, biophysics, bioengineering, or biochemistry courses.

SUPPLEMENTAL MATERIAL

A supplemental figure for Background on the Thermodynamics of Phase Separation is available at: https://doi.org/10.35459/tbp.2019.000104.

ACKNOWLEDGMENTS

The authors thank the students of Physics 381 at the University of San Diego who completed this lab module. Acknowledgment is made to the Donors of the American

Chemical Society Petroleum Research Fund for partial support of this research (57326-UNI10).

AUTHOR CONTRIBUTIONS

RM conceived and implemented the lab module for an experimental biophysics course. CPR took that course in the fall of 2017, performed experiments, and collected data. All authors wrote the manuscript.

REFERENCES

1. Hyman, A. A., and K. Simons. 2012. Beyond oil and water—phase transitions in cells. *Science* 337(6098):1047–1049.
2. Weber, S. C., and C. P. Brangwynne. 2012. Getting RNA and protein in phase. *Cell* 149(6):1188–1191.
3. Hyman, A. A., C. A. Weber, and F. Jülicher. 2014. Liquid-liquid phase separation in biology. *Annu Rev Cell Dev Biol* 30(1):39–58.
4. Brangwynne, C. P., P. Tompa, and R. V. Pappu. 2015. Polymer physics of intracellular phase transitions. *Nat Phys* 11(11):899–904.
5. Bergeron-Sandoval, L.-P., N. Safaee, and S. W. Michnick. 2016. Mechanisms and consequences of macromolecular phase separation. *Cell* 165(5):1067–1079.
6. Alberti, S. 2017. Phase separation in biology. *Curr Biol* 27(20):R1097–R1102.
7. Banani, S. F., H. O. Lee, A. A. Hyman, and M. K. Rosen. 2017. Biomolecular condensates: organizers of cellular biochemistry. *Nat Rev Mol Cell Biol* 18(5):285–298.
8. Shin, Y., and C. P. Brangwynne. 2017. Liquid phase condensation in cell physiology and disease. *Science* 357(6357):eaaf4382.
9. Uversky, V. N. 2017. Intrinsically disordered proteins in overcrowded milieu: membrane-less organelles, phase separation, and intrinsic disorder. *Curr Opin Struct Biol* 44:18–30.
10. Berry, J., C. P. Brangwynne, and M. Haataja. 2018. Physical principles of intracellular organization via active and passive phase transitions. *Rep Prog Phys* 81(4):046601.
11. Boeynaems, S., S. Alberti, N. L. Fawzi, T. Mittag, M. Polymenidou, F. Rousseau, J. Schymkowitz, J. Shorter, B. Wolozin, L. Van Den Bosch, P. Tompa, and M. Fuxreiter. 2018. Protein phase separation: a new phase in cell biology. *Trends Cell Biol* 28(6):420–435.
12. Itakura, A. K., R. A. Futia, and D. F. Jarosz. 2018. It pays to be in phase. *Biochemistry* 57(17):2520–2529.
13. Lee, C. F., and J. D. Wurtz. 2018. Novel physics arising from phase transitions in biology. *J Phys D Appl Phys* 52(2):023001.
14. Bentley, E. P., B. B. Frey, and A. A. Deniz. 2019. Physical chemistry of cellular liquid-phase separation. *Chemistry* 25(22):5600–5610.
15. Cable, J., C. Brangwynne, G. Seydoux, D. Cowburn, R. V. Pappu, C. A. Castañeda, L. E. Berchowitz, Z. Chen, M. Jonikas, A. Dernburg, T. Mittag, and N. L. Fawzi. 2019. Phase separation in biology and disease—a symposium report. *Ann N Y Acad Sci* 1452(1):3–11.
16. Elbaum-Garfinkle, S. 2019. Matter over mind: liquid phase separation and neurodegeneration. *J Biol Chem* 294:7160–7168.
17. Falahati, H., and A. Haji-Akbari. 2019. Thermodynamically driven assemblies and liquid–liquid phase separations in biology. *Soft Matter* 15:1135–1154.
18. Feng, Z., X. Chen, M. Zeng, and M. Zhang. 2019. Phase separation as a mechanism for assembling dynamic postsynaptic density signalling complexes. *Curr Opin Neurobiol* 57:1–8.
19. Nakashima, K. K., M. A. Vibhute, and E. Spruijt. 2019. Biomolecular chemistry in liquid phase separated compartments. *Front Mol Biosci* 6(21). doi: 10.3389/fmolb.2019.00021.
20. Perry, S. L. 2019. Phase separation: bridging polymer physics and biology. *Curr Opin Colloid Interface Sci* 39:86–97.
21. Turoverov, K. K., I. M. Kuznetsova, A. V. Fonin, A. L. Darling, B. Y. Zaslavsky, and V. N. Uversky. 2019. Stochasticity of biological soft matter: emerging concepts in intrinsically disordered proteins and biological phase separation. *Trends Biochem Sci* 44(8):716–728.
22. Hnisz, D., K. Shrinivas, R. A. Young, A. K. Chakraborty, and P. A. Sharp. 2017. A phase separation model for transcriptional control. *Cell* 169(1):13–23.
23. Zhou, H., S. Zhong, Z. Song, L. Zuo, Z. Qi, L.-J. Qu, and L. Lai. 2019. Mechanism of DNA-induced phase separation for transcriptional repressor VRN1. *Angew Chem* 131(15):4912–4916.
24. Riback, J. A., C. D. Katanski, J. L. Kear-Scott, E. V. Pilipenko, A. E. Rojek, T. R. Sosnick, and D. A. Drummond. 2017. Stress-triggered phase separation is an adaptive, evolutionarily tuned response. *Cell* 168(6):1028–1040. e1019.
25. Li, P., S. Banjade, H.-C. Cheng, S. Kim, B. Chen, L. Guo, M. Llaguno, J. V. Hollingsworth, D. S. King, S. F. Banani, P. S. Russo, Q.-X. Jiang, B. T. Nixon, and M. K. Rosen. 2012. Phase transitions in the assembly of multivalent signalling proteins. *Nature* 483(7389):336–340.
26. Oltsch, F., A. Klosin, F. Julicher, A. A. Hyman, and C. Zechner. 2019. Phase separation provides a mechanism to reduce noise in cells. bioRxiv: 524231, https:doi.org/10.1101/524231 (preprint posted 22 January 2019).
27. Gibson, B. A., L. K. Doolittle, L. E. Jensen, N. Gamarra, S. Redding, and M. K. Rosen. 2019. Organization and regulation of chromatin by intrinsic and regulated phase separation. *Cell* 179(2):470–424.
28. Turner, A. L., M. Watson, O. G. Wilkins, L. Cato, A. Travers, J. O. Thomas, and K. Stott. 2018. Highly disordered histone H1–DNA model complexes and their condensates. *Proc Natl Acad Sci U S A* 115(47):11964–11969.
29. Shin, Y., Y.-C. Chang, D. S. W. Lee, J. Berry, D. W. Sanders, P. Ronceray, N. S. Wingreen, M. Haataja, and C. P. Brangwynne. 2018. Liquid nuclear condensates mechanically sense and restructure the genome. *Cell* 175(6):1481–1491. e1413.
30. Strom, A. R., A. V. Emelyanov, M. Mir, D. V. Fyodorov, X. Darzacq, and G. H. Karpen. 2017. Phase separation drives heterochromatin domain formation. *Nature* 547(7662):241–245.
31. Larson, A. G., D. Elnatan, M. M. Keenen, M. J. Trnka, J. B. Johnston, A. L. Burlingame, D. A. Agard, S. Redding, and G. J. Narlikar. 2017. Liquid droplet formation by HP1α suggests a role for phase separation in heterochromatin. *Nature* 547(7662):236–240.
32. Bergeron-Sandoval, L.-P., and S. W. Michnick. 2018. Mechanics, structure and function of biopolymer condensates. *J Mol Biol* 430(23):4754–4761.
33. Benedek, G. B. 1997. Cataract as a protein condensation disease: the Proctor Lecture. *Invest Opthalmol Vis Sci* 38(10):1911–1921.
34. Simons, K., and E. Ikonen. 1997. Functional rafts in cell membranes. *Nature* 387(6633):569.
35. Cellular Mechanisms Driven By Liquid Phase Separation. EMBO/EMBL Symposium. Heidelberg, Germany. 11–14 May 2020. https://www.embo-embl-symposia.org/symposia/2020/EES20-04/index.html.
36. Brangwynne, C. P. 2019. Intracellular liquid condensates: new approaches to understand and control biomolecular phase transitions in living cells. In APS March Meeting 2019. Boston, MA, 4–8 March 2019. American Physical Society, College Park, MD.
37. Mullard, A. 2019. Biomolecular condensates pique drug discovery curiosity. *Nat Rev Drug Discov* 18:324.
38. Mitrea, D. M., B. Chandra, M. C. Ferrolino, E. B. Gibbs, M. Tolbert, M. R. White, and R. W. Kriwacki. 2018. Methods for physical characterization of phase-separated bodies and membrane-less organelles. *J Mol Biol* 430(23):4773–4805.
39. Wang, Z., G. Zhang, and H. Zhang. 2018. Protocol for analyzing protein liquid–liquid phase separation. *Biophys Rep* 5(1):1–9.
40. Uversky, V. N. 2019. Intrinsically disordered proteins and their "mysterious" (meta)physics. *Front Phys* 7:10.
41. Guzikowski, A. R., Y. S. Chen, and B. M. Zid. 2019. Stress-induced mRNP granules: form and function of processing bodies and stress granules. *Wiley Interdiscip Rev RNA* 10(3):e1524.
42. Jawerth, L. M., M. Ijavi, M. Ruer, S. Saha, M. Jahnel, A. A. Hyman, F. Jülicher, and E. Fischer-Friedrich. 2018. Salt-dependent rheology and surface tension of protein condensates using optical traps. *Phys Rev Lett* 121(25):258101.
43. Appleyard, D. C., K. Y. Vandermeulen, H. Lee, and M. J. Lang. 2006. Optical trapping for undergraduates. *Am J Phys* 75(1):5–14.
44. Rubinstein, M., and R. H. Colby. 2003. Polymer Physics. Oxford University Press, Oxford, UK.
45. Lee, C. F., C. P. Brangwynne, J. Gharakhani, A. A. Hyman, and F. Jülicher. 2013. Spatial organization of the cell cytoplasm by position-dependent phase separation. *Phys Rev Lett* 111(8):088101.
46. Berry, J., S. C. Weber, N. Vaidya, M. Haataja, and C. P. Brangwynne. 2015. RNA transcription modulates phase transition-driven nuclear body assembly. *Proc Natl Acad Sci U S A* 112(38):E5237–E5245.

47. Nott, T. J., E. Petsalaki, P. Farber, D. Jervis, E. Fussner, A. Plochowietz, T. D. Craggs, D. P. Bazett-Jones, T. Pawson, J. D. Forman-Kay, and A. J. Baldwin. 2015. Phase transition of a disordered nuage protein generates environmentally responsive membraneless organelles. *Mol Cell* 57(5):936–947.
48. Narayanan, A., A. Meriin, J. O. Andrews, J.-H. Spille, M. Y. Sherman, and I. I. Cisse. 2019. A first order phase transition mechanism underlies protein aggregation in mammalian cells. *eLife* 8:e39695.
49. McGorty, R. 2019. Python Code for Interactively Investigating Flory–Huggins Model. GitHub. Accessed 21 January 2020. https://github.com/rmcgorty/PhaseSeparation.
50. Hestenes, D. 1992. Modeling games in the Newtonian World. *Am J Phys* 60(8):732–748.
51. Schwarz, C. V., B. J. Reiser, E. A. Davis, L. Kenyon, A. Achér, D. Fortus, Y. Shwartz, B. Hug, and J. Krajcik. 2009. Developing a learning progression for scientific modeling: making scientific modeling accessible and meaningful for learners. *J Res Sci Teach* 46(6):632–654.
52. Zwickl, B. M., N. Finkelstein, and H. J. Lewandowski. 2014. Incorporating learning goals about modeling into an upper-division physics laboratory experiment. *Am J Phys* 82(9):876–882.
53. Hoskinson, A.-M., B. A. Couch, B. M. Zwickl, K. A. Hinko, and M. D. Caballero. 2014. Bridging physics and biology teaching through modeling. *Am J Phys* 82(5):434–441.
54. White, B. Y., A. Collins, and J. R. Frederiksen. 2011. The nature of scientific meta-knowledge. In Models and Modeling in Science Education. Models and Modeling: Cognitive Tools for Scientific Enquiry. M. S. Khine and I. M. Saleh, editors. Springer, Dordrecht, the Netherlands, pp. 41–76.
55. Krell, M., B. Reinisch, and D. Krüger. 2015. Analyzing students' understanding of models and modeling referring to the disciplines biology, chemistry, and physics. *Res Sci Educ* 45(3):367–393.
56. Strulson, C. A., R. C. Molden, C. D. Keating, and P. C. Bevilacqua. 2012. RNA catalysis through compartmentalization. *Nat Chem* 4(11):941–946.
57. Aumiller, W. M., B. W. Davis, and C. D. Keating. 2014. Chapter five—phase separation as a possible means of nuclear compartmentalization. In New Models of the Cell Nucleus: Crowding, Entropic Forces, Phase Separation, and Fractals. International Review of Cell and Molecular Biology. R. Hancock and K. W. Jeon, editors. Academic Press, Cambridge, MA, pp. 109–149.
58. Monterroso, B., S. Zorrilla, M. Sobrinos-Sanguino, C. D. Keating, and G. Rivas. 2016. Microenvironments created by liquid-liquid phase transition control the dynamic distribution of bacterial division FtsZ protein. *Sci Rep* 6:35140.
59. Tromp, R. H., A. R. Rennie, and R. A. L. Jones. 1995. Kinetics of the simultaneous phase separation and gelation in solutions of dextran and gelatin. *Macromolecules* 28(12):4129–4138.
60. Esquena, J. 2016. Water-in-water (W/W) emulsions. *Curr Opin Colloid Interface Sci* 25:109–119.
61. Elbaum-Garfinkle, S., Y. Kim, K. Szczepaniak, C. C.-H. Chen, C. R. Eckmann, S. Myong, and C. P. Brangwynne. 2015. The disordered P granule protein LAF-1 drives phase separation into droplets with tunable viscosity and dynamics. *Proc Natl Acad Sci U S A* 112(23):7189–7194.
62. Montgomery, T. S. H. 1898. Comparative cytological studies, with especial regard to the morphology of the nucleolus. *J Morphol* 15(2):265–582.
63. Dolgin, E. 2018. What lava lamps and vinaigrette can teach us about cell biology. *Nature* 555:300.
64. Brangwynne, C. P., C. R. Eckmann, D. S. Courson, A. Rybarska, C. Hoege, J. Gharakhani, F. Jülicher, and A. A. Hyman. 2009. Germline P granules are liquid droplets that localize by controlled dissolution/condensation. *Science* 324(5935):1729–1732.
65. Scalettar, B. A., and J. R. Abney. 2015. Biomedical imaging in the undergraduate physics curriculum: module on optical microscopy. *Am J Phys* 83(8):711–718.
66. Pluta, M. 1994. Nomarski's DIC microscopy: a review. In Phase Contrast and Differential Interference Contrast Imaging Techniques and Applications. M. Pluta and M. Szyjer, editors. International Society for Optics and Photonics, Bellingham, WA, pp. 10–25.
67. Webb, R. H. 1996. Confocal optical microscopy. *Rep Prog Phys* 59(3):427–471.
68. Banani, S. F., A. M. Rice, W. B. Peeples, Y. Lin, S. Jain, R. Parker, and M. K. Rosen. 2016. Compositional control of phase-separated cellular bodies. *Cell* 166(3):651–663.
69. Feric, M., N. Vaidya, T. S. Harmon, D. M. Mitrea, L. Zhu, T. M. Richardson, R. W. Kriwacki, R. V. Pappu, and C. P. Brangwynne. 2016. Coexisting liquid phases underlie nucleolar subcompartments. *Cell* 165(7):1686–1697.
70. Schindelin, J., I. Arganda-Carreras, E. Frise, V. Kaynig, M. Longair, T. Pietzsch, S. Preibisch, C. Rueden, S. Saalfeld, B. Schmid, J.-Y. Tinevez, D. J. White, V. Hartenstein, K. Eliceiri, P. Tomancak, and A. Cardona. 2012. Fiji: an open-source platform for biological-image analysis. *Nat Methods* 9(7):676–682.
71. Brangwynne, C. P., T. J. Mitchison, and A. A. Hyman. 2011. Active liquid-like behavior of nucleoli determines their size and shape in *Xenopus laevis* oocytes. *Proc Natl Acad Sci U S A* 108(11):4334–4339.
72. Wang, L., G. Zhang, H. Wu, J. Yang, and Y. Zhu. 2016. Note: a top-view optical approach for observing the coalescence of liquid drops. *Rev Sci Instrum* 87(2):026103.
73. Paulsen, J. D., R. Carmigniani, A. Kannan, J. C. Burton, and S. R. Nagel. 2014. Coalescence of bubbles and drops in an outer fluid. *Nat Commun* 5:3182.
74. Kavehpour, H. P. 2015. Coalescence of drops. *Annu Rev Fluid Mech* 47(1):245–268.
75. Lippincott-Schwartz, J., E. Snapp, and A. Kenworthy. 2001. Studying protein dynamics in living cells. *Nat Rev Mol Cell Biol* 2(6):444–456.
76. Axelrod, D., D. E. Koppel, J. Schlessinger, E. Elson, and W. W. Webb. 1976. Mobility measurement by analysis of fluorescence photobleaching recovery kinetics. *Biophys J* 16(9):1055–1069.
77. Goehring, N. W., D. Chowdhury, A. A. Hyman, and S. W. Grill. 2010. FRAP analysis of membrane-associated proteins: lateral diffusion and membrane-cytoplasmic exchange. *Biophys J* 99(8):2443–2452.
78. Röding, M., L. Lacroix, A. Krona, T. Gebäck, and N. Lorén. 2019. A highly accurate pixel-based FRAP model based on spectral-domain numerical methods. *Biophys J* 116(7):1348–1361.
79. Zhang, H., S. Elbaum-Garfinkle, E. M. Langdon, N. Taylor, P. Occhipinti, A. A. Bridges, C. P. Brangwynne, and A. S. Gladfelter. 2015. RNA controls polyQ protein phase transitions. *Mol Cell* 60(2):220–230.
80. Kaur, T., I. Alshareedah, W. Wang, J. Ngo, M. M. Moosa, and P. R. Banerjee. 2019. Molecular crowding tunes material states of ribonucleoprotein condensates. *Biomolecules* 9(2):71.
81. Koulouras, G., A. Panagopoulos, M. A. Rapsomaniki, N. N. Giakoumakis, S. Taraviras, and Z. Lygerou. 2018. EasyFRAP-web: a web-based tool for the analysis of fluorescence recovery after photobleaching data. *Nucleic Acids Res* 46(W1):W467–W472.
82. Kruglak, H. 1989. Boltzmann's constant: a laboratory experiment. *Am J Phys* 57(3):216–217.
83. Nakroshis, P., M. Amoroso, J. Legere, and C. Smith. 2003. Measuring Boltzmann's constant using video microscopy of Brownian motion. *Am J Phys* 71(6):568–573.
84. Catipovic, M. A., P. M. Tyler, J. G. Trapani, and A. R. Carter. 2013. Improving the quantification of Brownian motion. *Am J Phys* 81(7):485–491.
85. Langbeheim, E., S. Livne, S. A. Safran, and E. Yerushalmi. 2011. Introductory physics going soft. *Am J Phys* 80(1):51–60.